

Multi-Object Near-IR $H\alpha$ Spectroscopy of $z \sim 1$ star-forming galaxies in the HDF-N

Michelle Doherty^{1*}, Andrew Bunker^{1,2}, Robert Sharp^{1,3}, Gavin Dalton⁴,
Ian Parry¹, Ian Lewis⁴, Emily MacDonald⁴, Christian Wolf⁴ & Hans Hippelein⁵

¹*Institute of Astronomy, Madingley Road, Cambridge, CB3 0HA, UK*

²*School of Physics, University of Exeter, Stocker Road, Exeter, UK*

³*Anglo-Australian Observatory, Sydney, Australia*

⁴*Astrophysics, NAPL, Keble Road, Oxford, OX1 3RH, UK*

⁵*MPIA, Heidelberg*

Released 2004? Xxxxx XX

ABSTRACT

We present preliminary results from a programme to obtain multi-object near-infrared spectroscopy of galaxies at redshifts $0.7 < z < 1.5$. We are using the instrument CIRPASS (the Cambridge Infra-Red PANoramic Survey Spectrograph), in multi-object mode, to survey $H\alpha$ in galaxies at $z \sim 1$. We aim to address the true star formation history of the universe at this epoch: potentially the peak period of star formation activity. $H\alpha$ is the same star formation measure used at low redshift, and hence we can trace star formation without the systematic uncertainties of using different calibrators in different redshift bins, or the extreme dust extinction in the rest-UV. CIRPASS has been successfully demonstrated in multi-object mode on the AAT and WHT. Here we present preliminary results from one of our fields, the Hubble Deep Field North, observed with the WHT. With 150 fibres deployed over an unvignetted field of ~ 15 arcmin, we have several detections of $H\alpha$ from star forming galaxies at $0.8 < z < 1.0$ and present spectra of the seven brightest of these. By pre-selecting galaxies with redshifts such that $H\alpha$ will appear between the OH sky lines, we can detect star formation rates of $5 h_{70}^{-2} M_{\odot} \text{ yr}^{-1}$ (5σ in 3-hours, $\Omega_M = 0.3$, $\Omega_{\Lambda} = 0.7$). It appears that star formation rates inferred from $H\alpha$ are, on average, a factor of more than two higher than those based on the UV continuum alone.

Key words: instrumentation: spectrographs – galaxies: evolution – galaxies: formation – galaxies: high-redshift

1 INTRODUCTION

A central problem in observational cosmology is determining at which epoch the majority of stars formed. This has important implications for models of galaxy formation and evolution. Despite recent progress in this area, the star formation history of the universe is still a topic of intense debate. There is substantial evidence that the star formation rate was much higher in the recent past, compared with the current epoch, rising steeply to $z \sim 1$ (e.g. Lilly et al. 1996, Tresse et al. 2002, Hippelein et al. 2003). However, it is still unclear whether at higher redshifts the star formation density declines, plateaus or perhaps continues to slowly increase. Most quantitative attempts to measure the global

star formation history have suffered from having to use different indicators of star formation in various redshift bins (Madau et al., 1996), redshifted into the optical. These various indicators not only have uncertain relative calibration but are also affected differently by dust extinction. To make a reliable comparison, the same tracer of star formation must be used at high redshift as that used locally. The $H\alpha$ emission line is a good tracer of the *instantaneous* star formation rate, and has been widely used in surveys at low redshift. It is particularly suitable as it is relatively immune to metallicity effects and is much less susceptible to extinction by dust than the rest-UV continuum and Lyman- α (which is also selectively quenched through resonant scattering). It is also important to use $H\alpha$ to calibrate secondary indicators of star formation such as [OII]3727Å, which are often used at redshift one. However, tracing $H\alpha$ to early epochs forces a move to the near-IR at $z > 0.6$. The recent advent of good infra-

* E-mail: md@ast.cam.ac.uk

red spectrographs on large telescopes has facilitated rapid advancement in this area, with observations of a few tens of galaxies at $z \sim 1$ (e.g. Tresse et al., 2002, Glazebrook et al., 1999) and $z \sim 2$ (Erb et al., 2003). However, until recently, near-infrared spectroscopy has been restricted to long-slit work and building samples using single object spectroscopy is inefficient in terms of telescope time. The small statistical samples obtained result in large uncertainties in the global properties of galaxies at $z \sim 1$. There has been successful “multi-object” spectroscopy through slitless surveys in the near-infrared from space (the HST/NICMOS survey of Yan et al. 1999), but such an approach has poor sensitivity because of the high background. It is only now that true multi-object infrared spectroscopy is possible from the ground, using either a slitmask approach (e.g. IRIS2 and FLAMINGOS) or a fibre-fed spectrograph. In this paper we present the first successful demonstration of multi-object near-infrared spectroscopy of high-redshift galaxies.

We have used our fibre-fed CIRPASS spectrograph (Cambridge InfraRed PANoramic Survey Spectrograph, Parry et al. 2000) to measure the star formation rates of a sample of galaxies in Hubble Deep Field North (HDF-N) (Williams et al., 1996). This is the initial stage of a larger survey to address the true star formation history of the universe at redshifts $z = 0.7 - 1.5$, through $H\alpha$ measurements of several hundred galaxies. CIRPASS can operate with a 150 fibre multi-object bundle, with the ability to simultaneously observe 75 object+sky targets. It thus offers a huge multiplex advantage, compared with surveys utilising single object spectroscopy - of which the largest to date is the work of Tresse et al. (2002), which surveys a total of 33 galaxies. Controlled selection of our targets ensures an accurate knowledge of the completeness of our survey. The selection function will be discussed in a future paper (Doherty et al., 2004, *in prep.*).

In this paper, we focus on the $H\alpha$ detections from our pilot study of galaxies at $z \sim 1$ in the HDF-N with CIRPASS. The layout of the paper is as follows: in section 2 we describe the instrument and our observations and in section 3 we detail the data reduction techniques employed. In section 4 we present results for a sub-sample of objects, which constitute our brightest detections of $H\alpha$ (with $S/N > 5\sigma$), and use the results to derive the star formation rates in these redshift one galaxies, comparing these with that inferred from the rest-frame UV (2400Å) continuum. Our conclusions are presented in section 5.

In this paper we adopt the standard “concordance” cosmology of $\Omega_M = 0.3$, $\Omega_\Lambda = 0.7$, and use $h_{70} = H_0/70 \text{ km s}^{-1} \text{ Mpc}^{-1}$. AB magnitudes (Oke & Gunn, 1983) are used throughout.

2 OBSERVATIONS

We performed multi-object spectroscopy of galaxies in the vicinity of the HDF-N with CIRPASS, a near-infrared fibre-fed spectrograph operating between 0.9 and 1.67 μm . The upper cut-off is set by a blocking filter which reduces the thermal background. These HDF-N observations were undertaken at the cassegrain focus on the 4.2 m William Herschel Telescope (WHT) in La Palma. The instrument was used in multi-object mode, with 150 fibres of 1.1” diam-

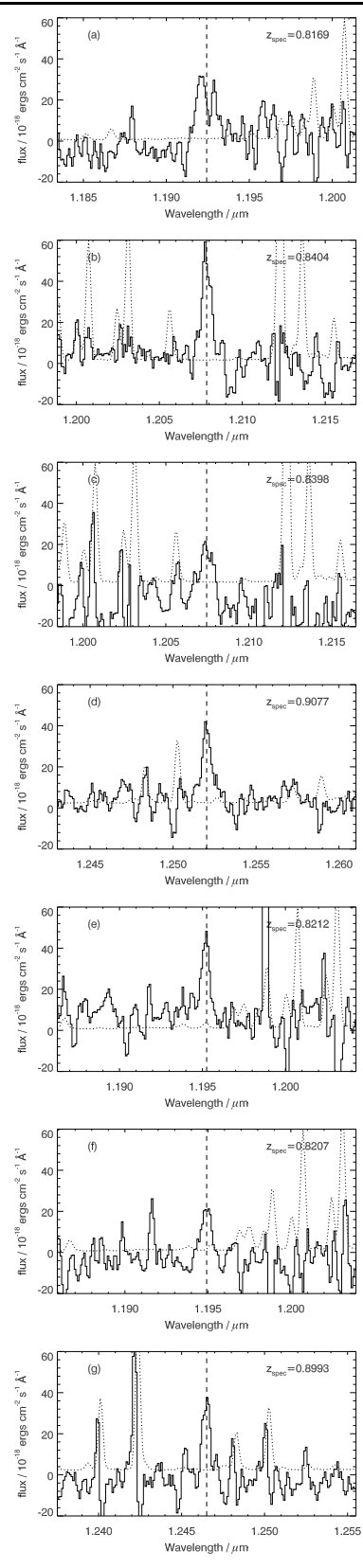


Figure 1. Spectra for the 7 brightest $H\alpha$ detections in our sample. The expected position of $H\alpha$ at the optical spectroscopic redshift is marked with a dashed line. The sky spectrum is overlaid in dotted lines. The emission lines all fall well between sky lines.

eter on the sky (comparable to the expected seeing convolved with typical galaxy profiles). These fibres are deployable over an unvignetted field of diameter $15'$. We used the FOCAP mechanism developed by the AAO as an interface to the telescope, with holes drilled in a brass plate to hold fibres in position. We acquired the field using six guide bundles, each containing seven closely packed fibres, centred on bright stars. We thus centroided the plate to an accuracy better than $0.5''$, that is, less than half the fibre size.

A Hawaii 2K detector was used, and a grating of 831 lines/mm, producing a dispersion of $0.95\text{\AA}/\text{pixel}$. The FWHM of each fibre extends over 2.7 pixels in both the spatial and spectral domain. The wavelength coverage was 1726\AA , covering most of the J-band, and the grating was tilted to set a central wavelength of $\lambda_c = 1.25\mu\text{m}$. The resolving power was $R = \lambda/\Delta\lambda_{FWHM} \approx 5000$. At this resolution the background is very dark between the OH sky lines in the J- and H-bands, with only about 10% of the array contaminated by skylines. By targeting galaxies with redshifts which place the $\text{H}\alpha$ emission lines between the skylines we become very sensitive to line emission – indeed, we are limited by the instrument background (although it is cooled to -42°C) rather than the sky. We targeted 65 objects using pairs of fibres offset by $6'$, nodding the telescope between the A and B positions such that the fibre pairs alternately received light from the target object and sky. The 2D data frames are then subtracted directly from each other before extracting the spectra, so that sky subtracted off has been observed down the same fibre as the object. Although the sky background varies a lot on timescales equivalent to our exposure time, we achieved reasonable first order sky subtraction. Some low throughput fibres were not allocated positions. A total of 12 hours integration time was obtained, over 3 nights, with individual integrations of 30 or 40 minutes per pointing. The array was read out non-destructively every 10 minutes, with three or four such loops per pointing to allow for cosmic ray rejection. There were 10 reads per each 10 minute loop to reduce the readout noise, ensuring that we achieved background-limited observations.

The majority of our targets in this field were selected from the redshift survey of the HDF-N and “flanking fields” carried out by Cohen et al. (2000), which is $> 92\%$ complete to $R_{AB} = 24$ for objects in the HDF-N proper and $R_{AB} = 23$ in the flanking fields. We selected all $R_{AB} < 24.5$ targets within the redshift range $0.73 < z < 1.0$ which fell within our $15'$ unvignetted field of view. A handful of objects were removed because of the limit on the fibre spacing (a minimum of $20''$). We redefined the coordinates of our targets based on the GOODSv1.0 system (Giavalisco et al., 2003), for consistency in our astrometry between the targets and the alignment stars. The completeness of our sample is discussed in Doherty et al. (2004, in preparation). In this paper we present observations of the seven sources in HDF-N where $\text{H}\alpha$ was detected at more than 5σ . These sources are all in the Cohen et al. (2000) flanking field, with $R_{AB} < 23.0$.

3 DATA REDUCTION

Data reduction was performed under IRAF with the CIRPASS package¹. For each multiple read exposure, the average of each loop was subtracted from the average of the next loop of non-destructive reads to form sub-integrations of 10 minutes each at the same pointing. These sub-integrations were then averaged together using the `crreject` algorithm to reject cosmic ray strikes (using limits of 3σ according to gain and readnoise). The frames were then beam-switched by taking A-B pairs (providing first-order sky subtraction). We then subtracted of the average residual bias, determined from the unilluminated region of the array (the bias level of infrared arrays is known to float with time). The spectrum in each fibre was then optimally extracted according to the prescription of Johnson et al. (2002), that is, the fibres were profile fitted in triplets (central fibre and two adjacent fibres) and the pixel values weighted and summed. This removes the contribution from the two adjacent fibres to the central fibre. This process produced positive (object-sky) and negative (sky-object) fibre pairs.

Dome flat fields were also optimally extracted and used to correct variations in the fibre throughput and the spectral response of pixels on the array. Wavelength calibration was performed using an argon arc, fitting 30 lines with a third order polynomial, resulting in an rms dispersion of 0.1\AA . The spectra were then rectified to lie on a common wavelength scale.

In order to remove sky residuals which did not fully subtract out in the beam-switch, a low order polynomial was fitted and subtracted along each rectified column of the flat-fielded, extracted spectra. This removed residuals due to temporal variation of the night sky spectrum. Flux calibration was carried out using observations of a $J = 10.68$ magnitude star from 2MASS which was placed on the same HDF-N plate as our targets. As it was thus observed simultaneously, this also corrects for temporal changes in the seeing, which fluctuated a lot over the course of the observations. As a consistency check we looked at 6 bright stars placed on the plate in another field from the survey. The fluxes were consistent to within 3%, comparing the counts in our CIRPASS spectra with those predicted from the 2MASS J -band magnitudes.

In an average fibre, between skylines, for a spectrally unresolved line ($< 60\text{km s}^{-1}$) we achieve a sensitivity of $7.2 \times 10^{-17}\text{erg s}^{-1}\text{cm}^{-2}$ at 5σ in 3 hours. However the emission lines we detect are typically broader than this ($\sim 100 - 250\text{ km s}^{-1}$, Table 1).

4 RESULTS

In this paper we analyse a sub-sample of our HDF-N data: those galaxies with strongly detected (greater than 5σ) $\text{H}\alpha$ emission. These emission line spectra are shown in Figure 1. The spectrum of the night sky is overlaid in dotted lines, giving a clear indication of the positions of skyline residuals, where the noise is significantly higher due to the enhanced background counts. These residuals do not adversely affect

¹

http://www.ast.cam.ac.uk/~optics/cirpass/docs/install_cirp_software.html

the data as the emission lines shown here all fall well between skylines. The dashed line shows the expected position for $H\alpha$, given the optical spectroscopic redshift. The centroid of $H\alpha$ is accurate to 2 pixels ($\approx 2\text{\AA}$), so the error on the redshift is less than 0.001. There is agreement at this level with the optical redshifts given in Cohen et al. (2000) and which are listed in Column 5 of Table 1.

We accurately measured the integrated line fluxes by measuring between zero power points (Table 1), having first subtracted off a continuum fit derived from regions adjacent to the emission line and unaffected by skylines. We checked our flux measurements by also fitting gaussian profiles to the lines, finding consistent values. The gaussian fits also gave the full width at half maximum (FWHM) for each line (Table 1). After subtracting the instrumental resolution in quadrature from the galaxy line widths, we find velocity FWHMs for these galaxies in the range $\sim 100 - 250 \text{ km s}^{-1}$, equivalent to $\sigma_{1D} = 40 - 100 \text{ km s}^{-1}$. We note that some of this velocity width may be due to galactic rotation in the extended galaxies (galaxies J1236175+6214027, J1237084+6215150 and J1237166+6210424 are the most spatially extended and also exhibit the broadest lines).

The $H\alpha$ luminosity of a galaxy is directly proportional to the ionising flux from massive stars, which drops off very quickly, about 20 million years after star formation ceases. $H\alpha$ thus traces the instantaneous star formation rate, whereas the UV luminosity evolves in time with the changes in stellar population and continues to rise even after star formation has ended. Since the $H\alpha$ flux is proportional to the number of OB stars, in order to extrapolate to a total star formation rate (SFR) it is necessary to assume an initial mass function (IMF), and the conversion from $H\alpha$ flux to SFR is quite sensitive to the IMF assumed (see discussion in Glazebrook et al. 1999). We use Kennicutt's (1998) conversion which assumes a Salpeter IMF with $0.1 M_{\odot} < M < 100 M_{\odot}$:

$$\text{SFR}(M_{\odot} \text{ yr}^{-1}) = 7.9 \times 10^{-42} L_{H\alpha} (\text{erg s}^{-1}) \quad (1)$$

The derived SFRs of the galaxies are shown in Table 2, and in Figure 3 we show B , V , i' and z' band images from HST/ACS taken from GOODS v1.0 (Giavalisco et al., 2003). We performed photometry on these images with $1''$ apertures, for consistency with our infra-red fibre size. In most cases the $1.1''$ fibres enclose most of the B-band light. However, for three of the sources (galaxies J1236175+6214027, J1237084+6215150 and J1237166+6210424) some fraction ($< 20\%$) is missed. We reiterate that we have compensated for the effects of seeing by placing one of the fibres on a bright star in the field (thus observing the star simultaneously with the galaxies). This allows us to correct the flux calibration for seeing dependant aperture losses.

We used the B band magnitudes (4500\AA) to calculate rest frame UV (2400\AA) flux densities and corresponding star formation rates. These are also shown in Table 2. For consistency, we also use the conversion given in Kennicutt (1998):

$$\text{SFR}(M_{\odot} \text{ yr}^{-1}) = 1.4 \times 10^{-28} L_{\nu} (\text{erg s}^{-1} \text{ Hz}^{-1}) \quad (2)$$

assuming the same IMF as used when deriving SFRs from the $H\alpha$ flux (Equation 1). The UV SFR relation also assumes continuous star formation over $\sim 10^8$ years.

Figure 2 shows the SFRs for each galaxy calculated using the UV luminosity density and the $H\alpha$ flux: those cal-

culated from the UV luminosity densities are a factor of two lower on average, than those from $H\alpha$. This is probably due to the differential effect of dust extinction in the redshift one galaxies between $\lambda_{\text{rest}} \approx 2400\text{\AA}$ and 6563\AA . This is consistent with results obtained by Glazebrook et al. (1999), Tresse et al. (2002), and Yan et al. (1999) who all find $\text{SFR}(H\alpha)/\text{SFR}(\text{UV})$ ratios of around 2-3.

There is no uniform correction that can be applied to the SFR estimated from UV flux in order to derive the true star formation rate: the amount of extinction varies in each object due to inherent differences in physical properties of the galaxies (e.g. (Sullivan et al., 2001)). As can be seen in Figure 2, the statistical errors in our $H\alpha$ flux measurements are not great enough to account for the scatter, which instead is attributable to different dust extinctions in our galaxy sample. $H\alpha$ provides a more robust indicator for SFR, giving an independent estimate that is much less affected by dust obscuration. The ratio of the total $\text{SFR}_{H\alpha}$ to SFR_{UV} for this sub-sample is 2. This fraction is potentially biased high, as there is a selection effect in this sub-sample due to the fact that we are only including the sources with strong detections of $H\alpha$: we will address the full R -band magnitude-limited sample in a future paper.

We now estimate the true star formation rate for each galaxy, assuming that the Kennicutt (1998) relations for $H\alpha$ and UV SFRs should yield the same extrinsic SFR in the absence of extinction (i.e. assuming a Salpeter IMF and continuous star formation). Furthermore, we assume a Calzetti dust extinction law, appropriate for starburst galaxies (Calzetti, 1997). For each galaxy we calculate the reddening value $E(B-V)$ which gives the observed $\text{SFR}(H\alpha)/\text{SFR}(\text{UV})$ ratio. In Table 2 we list the reddening values derived and use these to compute the total dust corrected star formation rates. These are typically 50% higher than those based purely on $H\alpha$, corresponding to an average $E(B-V) = 0.16$. Hence surveys based solely on UV (e.g. 2400\AA) continua (without dust correction) will underestimate SFRs at redshift one by factors of $\approx 2 - 11$.

5 CONCLUSION

We have performed multi-object, near-infrared spectroscopy of $z \sim 1$ galaxies in the Hubble Deep Field North, using CIRCASS-MOS. These observations are part of an on-going survey to trace star formation rates at redshift one. We have presented our brightest detections of $H\alpha$ from three hours of observing time, as a demonstration of the success of this technique. We have shown that we can detect $H\alpha$ at sufficient signal to noise to obtain a good estimate of star formation rates in these galaxies. By pre-selecting galaxies with $H\alpha$ redshifted between the OH sky lines, we can detect star formation rates of $5 h_{70}^{-2} M_{\odot} \text{ yr}^{-1}$ (5σ in 3-hours). The star formation rates obtained are higher than those estimated from UV continuum by a factor of about two, due to dust obscuration in the UV. This is consistent with previous work in this area. We have another ~ 60 sources in this field, at known redshifts, therefore by stacking the spectra we will be able to obtain a global star formation rate for $z \sim 1$ galaxies in the vicinity of the HDF-N. Between this and other fields we hope to build up a sample of several hundred galaxies which will allow us to determine the $H\alpha$ luminosity function

id	name	RA (J2000)	Dec (J2000)	$\lambda_{H\alpha}$ (Å)	z_{opt}	$z_{H\alpha}$	fwhm (Å)	Vel. FWHM km s ⁻¹	flux $\times 10^{-16}$ erg s ⁻¹ cm ⁻²
(a)	J1236175+6214027	12 36 17.536	+62 14 02.70	11924	0.818	0.8169	*	*	3.60 ± 5.58
(b)	J1237063+6215185	12 37 06.293	+62 15 18.50	12078	0.84	0.8404	5.9	127	3.31 ± 0.38
(c)	J1237084+6215150	12 37 08.381	+62 15 15.04	12074	0.839	0.8398	11.1	259	3.01 ± 0.54
(d)	J1237087+6211285	12 37 08.659	+62 11 28.52	12520	0.907	0.9077	5.8	124	2.54 ± 0.34
(e)	J1237141+6210448	12 37 14.141	+62 10 44.78	11952	0.821	0.8212	4.8	97	2.27 ± 0.36
(f)	J1237166+6210424	12 37 16.631	+62 10 42.36	11949	0.821	0.8207	6.6	146	1.78 ± 0.40
(g)	J1237167+6213105	12 37 16.716	+62 13 10.54	12465	0.898	0.8993	5.5	116	2.63 ± 0.31

Table 1. Measured properties of the H α emission lines in our $> 5\sigma$ detections in the HDF-N. The optical redshifts are from Cohen et al. (2000). The H α line in J1236175+6214027 is not well fit by a gaussian profile, so no FWHM is reported.

id	R_{AB} mag	SFR _{Hα} M _⊙ yr ⁻¹	B_{AB} mag	flux density L_{ν} 10 ²⁸ erg s ⁻¹ Hz ⁻¹	SFR _{UV} M _⊙ yr ⁻¹	ratio SFR _{Hα} /SFR _{UV}	E(B-V) mag	SFR _{tot} M _⊙ yr ⁻¹ (dust corrected)
(a)	21.73	9.0	23.89	1.76	2.5	3.6	0.30	28.7
(b)	22.22	8.9	22.89	4.70	6.6	1.3	0.07	11.9
(c)	21.62	8.0	23.44	2.81	3.9	2.0	0.17	15.4
(d)	22.23	8.3	23.23	4.00	5.6	1.5	0.10	12.2
(e)	22.32	5.7	23.32	3.01	4.2	1.4	0.09	8.1
(f)	21.59	4.5	23.85	1.85	2.6	1.7	0.13	7.5
(g)	22.72	8.4	23.96	2.01	2.8	3.0	0.25	22.1

Table 2. Identification, R_{AB} magnitude (Cohen et al., 2000), SFR derived from H α , HST B-band magnitude (1'' aperture) and corresponding flux density and SFR_{uv} for our $> 5\sigma$ detections.

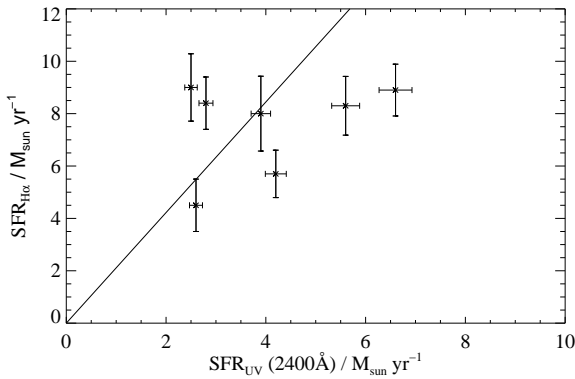


Figure 2. Comparison of SFRs obtained from UV continuum flux at 2400 Å versus H α flux for the individual galaxies. The SFRs derived from UV luminosity are consistently underestimated. The solid line has a gradient of 2.11 and represents the line of best fit to the data (using a least squares fit). The errors in the SFR(H α) values reflect the errors in the flux calibration. We assume $\sim 5\%$ error in the UV flux, which is dominated by errors in positioning the fibres (i.e. mirrored in the exact positioning of the aperture for the B_{AB} magnitude.)

at $z \sim 1$ and hence address the true star formation rate at this important epoch. The success of our pilot multi-object spectroscopic survey bodes well for future instruments, such as FMOS on Subaru.

ACKNOWLEDGMENTS

This paper is based on observations obtained at the William Herschel Telescope, which is operated by the Isaac Newton

Group on behalf of the UK Particle Physics and Astronomy Research Council. We thank the WHT staff, in particular Danny Lennon, Kevin Dee, Rene Ruten, Juerg Rey and Carlos Martin, for their help and support in enabling CIRPASS to be used as a visitor instrument. Simon Hodgkin, Elizabeth Stanway and Paul Allen all assisted in obtaining the observations. CIRPASS was built by the instrumentation group of the Institute of Astronomy in Cambridge, UK. We thank the Raymond and Beverly Sackler Foundation and PPARC for funding this project. We are indebted to Dave King, Jim Pritchard, Anthony Horton & Steve Medlen for contributing their instrument expertise. We are grateful to Steve Lee and Stuart Ryder at AAO for assistance in designing the fibre plug plates, and thank the AAO for the use of the FOCAP fibre unit. The optimal extraction software for this fibre spectroscopy was written by Rachel Johnson, Rob Sharp and Andrew Dean. This research is also partially based on observations with the NASA/ESA *Hubble Space Telescope*, obtained at the Space Telescope Science Institute (STScI), which is operated by AURA under NASA contract NAS 5-26555. These observations are associated with proposals #9425 & 9583 (the GOODS public imaging survey). We also used results from the Caltech Faint Galaxy Redshift Survey in the HDF-N, and thank Judy Cohen and colleagues for making these catalogues publically available. MD is grateful for support from the Fellowship Fund Branch of AFUW Qld Inc., the Isaac Newton Studentship, the Cambridge Commonwealth Trust and the University of Sydney. ECM acknowledges the C.K. Marr Educational Trust.

REFERENCES

Calzetti D., 1997, in American Institute of Physics Conference

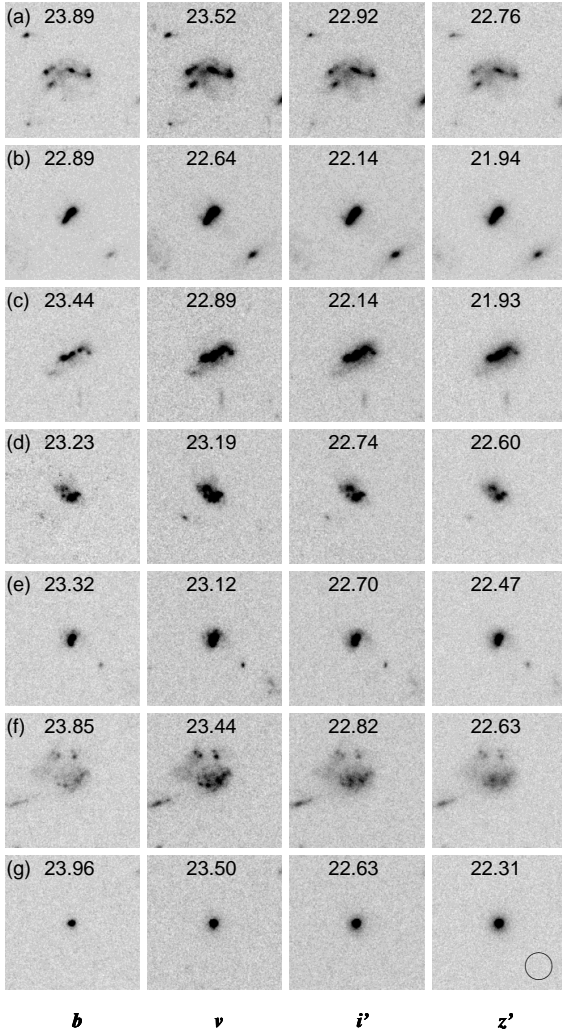


Figure 3. Postage stamp images of the objects showing H α emission listed in Table 1, with corresponding identifications. Images are taken from the B,V,i',z' bands in the GOODS v1 images. The image size is 5'' to a side. AB magnitudes for 1'' apertures (to match the fibre size) in each band are shown at the top of each image. The size of the fibre on the sky is shown by a circle in the bottom right corner of the stack of images.

Lilly S. J., Le Fevre O., Hammer F., Crampton D., 1996, ApJ, 460, L1
Madau P., Ferguson H. C., Dickinson M. E., Giavalisco M., Steidel C. C., Fruchter A., 1996, MNRAS, 283, 1388
Oke J. B., Gunn J. E., 1983, ApJ, 266, 713
Parry I. R., Mackay C. D., Johnson R. A., McMahon R. G., Dean A., Ramaprakash A. N., King D. L., Pritchard J. M., Medlen S. R., Sabbey C. S., Ellis R. S., Aragon-Salamanca A., 2000, in Proc. SPIE Vol. 4008, p. 1193-1202, Optical and IR Telescope Instrumentation and Detectors, Masanori Iye; Alan F. Moorwood; Eds. CIRPASS: a NIR integral field and multi-object spectrograph. pp 1193-1202
Sullivan M., Mobasher B., Chan B., Cram L., Ellis R., Treyer M., Hopkins A., 2001, ApJ, 558, 72
Tresse L., Maddox S. J., Le Fèvre O., Cuby J.-G., 2002, MNRAS, 337, 369
Williams R. E., Blacker B., Dickinson M., Dixon W. V. D., Ferguson H. C., Fruchter A. S., Giavalisco M., Gilliland R. L., Heyer I., Katsanis R., Levay Z., Lucas R. A., McElroy D. B., Petro L., Postman M., Adorf H., Hook R., 1996, AJ, 112, 1335
Yan L., McCarthy P. J., Freudling W., Teplitz H. I., Malumuth E. M., Weymann R. J., Malkan M. A., 1999, ApJ, 519, L47

Series UV Opacity in Nearby Galaxies and Application to Distant Galaxies. p. 403
Cohen J. G., Hogg D. W., Blandford R., Cowie L. L., Hu E., Songaila A., Shopbell P., Richberg K., 2000, ApJ, 538, 29
Erb D. K., Shapley A. E., Steidel C. C., Pettini M., Adelberger K. L., Hunt M. P., Moorwood A. F. M., Cuby J., 2003, ApJ, 591, 101
Giavalisco M., GOODS Team 2003, American Astronomical Society Meeting, 202,
Glazebrook K., Blake C., Economou F., Lilly S., Colless M., 1999, MNRAS, 306, 843
Hippelein H., Maier C., Meisenheimer K., Wolf C., Fried J. W., von Kuhlmann B., Kümmel M., Phleps S., Röser H.-J., 2003, A&A, 402, 65
Johnson R. A., Dean A. J., Parry I. R., 2002, in ASP Conf. Ser. 282: Galaxies: the Third Dimension Extracting IFU Spectra. p. 531
Kennicutt R. C., 1998, ARA&A, 36, 189